Neurochemistry International 123 (2019) 22–33

Contents lists available at ScienceDirect

Neurochemistry International

journal homepage: www.elsevier.com/locate/neuint

Selective deletion of glutamine synthetase in the mouse cerebral cortex induces glial dysfunction and vascular impairment that precede epilepsy and neurodegeneration

Yun Zhou[a,*], Roni Dhaher[b], Maxime Parent[c], Qiu-Xiang Hu[a], Bjørnar Hassel[d], Siu-Pok Yee[e], Fahmeed Hyder[c], Shaun E. Gruenbaum[b], Tore Eid[a,b,**], Niels Christian Danbolt[a,***]

[a] Neurotransporter Group, Department of Molecular Medicine, Institute of Basic Medical Sciences, University of Oslo, N-0317, Oslo, Norway
[b] Department of Laboratory Medicine, Yale School of Medicine, New Haven, CT, 06520, USA
[c] Magnetic Resonance Research Center, Yale School of Medicine, New Haven, CT, 06520, USA
[d] Department of Complex Neurology and Neurohabilitation, Oslo University Hospital, University of Oslo, N-0450, Oslo, Norway
[e] Department of Cell Biology, University of Connecticut Health, Farmington, CT, 06030, USA

ARTICLE INFO

Keywords:
Cerebrovascular dysfunction
Epilepsy
Glul
Neurodegeneration
Metabolism
Gliopathy

ABSTRACT

Glutamate-ammonia ligase (glutamine synthetase; Glul) is enriched in astrocytes and serves as the primary enzyme for ammonia detoxification and glutamate inactivation in the brain. Loss of astroglial Glul is reported in hippocampi of epileptic patients, but the mechanism by which Glul deficiency might cause disease remains elusive. Here we created a novel mouse model by selectively deleting Glul in the hippocampus and neocortex. The Glul deficient mice were born without any apparent malformations and behaved unremarkably until postnatal week three. There were reductions in tissue levels of aspartate, glutamate, glutamine and GABA and in mRNA encoding glutamate receptor subunits GRIA1 and GRIN2A as well as in the glutamate transporter proteins EAAT1 and EAAT2. Adult Glul-deficient mice developed progressive neurodegeneration and spontaneous seizures which increased in frequency with age. Importantly, progressive astrogliosis occurred before neurodegeneration and was first noted in astrocytes along cerebral blood vessels. The responses to CO_2-provocation were attenuated at four weeks of age and dilated microvessels were observed histologically in sclerotic areas of cKO. Thus, the abnormal glutamate metabolism observed in this model appeared to cause epilepsy by first inducing gliopathy and disrupting the neurovascular coupling.

1. Introduction

Glutamate-ammonia ligase (glutamine synthetase; Glul) is enriched in astrocytes (Martinez-Hernandez et al., 1977) and plays a critical role in the conversion of glutamate to glutamine and thereby also in the removal of neurotoxic ammonia in the central nervous system (CNS). Because treatment of rodents with the Glul inhibitor methionine sulfoximine induces convulsive seizures (Eid et al., 2016) and because Glul is deficient in parts of the hippocampus in patients with mesial temporal lobe epilepsy (MTLE) (Eid et al., 2004; van der Hel et al., 2005), a role for Glul in epileptogenesis has been proposed. Consistent with this idea, the few described patients suffering from congenital Glul

Abbreviations: CAS, Chemical Abstracts Service Registry Number; CVR, cerebrovascular reactivity; Glul, glutamate-ammonia ligase (a.k.a. glutamine synthetase, GS); cKO, conditional knockout; Cre, Cyclization recombinase; EAATs, excitatory amino acid transporters; EEG, electroencephalogram; EAAC1, excitatory amino acid carrier (EAAT3, slc1a1); GLAST, glutamate aspartate transporter (EAAT1, slc1a3); EAAT2, glutamate transporter 2 (EAAT2, slc1a2); GFAP, glial fibrillary acidic protein; fMRI, functional MRI; MRI, magnetic resonance imaging; MTLE, mesial temporal lobe epilepsy; NaPi, sodium phosphate buffer at pH 7.4; NCS, newborn calf serum; SDS, sodium dodecyl sulfate; WT, wild-type in the sense that the Glul gene is intact

* Corresponding author. Neurotransporter Group, Department of Molecular Medicine, Institute of Basic Medical Sciences, University of Oslo, N-0317, Oslo, Norway.
** Corresponding author. Department of Laboratory Medicine, Yale School of Medicine, New Haven, CT, 06520, USA.
*** Corresponding author. Neurotransporter Group, Department of Molecular Medicine, Institute of Basic Medical Sciences, University of Oslo, N-0317, Oslo, Norway.
E-mail addresses: yun.zhou@medisin.uio.no (Y. Zhou), tore.eid@yale.edu (T. Eid), n.c.danbolt@medisin.uio.no (N.C. Danbolt).
URL: http://neurotransporter.org (N.C. Danbolt).

https://doi.org/10.1016/j.neuint.2018.07.009
Received 4 June 2018; Received in revised form 22 July 2018; Accepted 23 July 2018
Available online 24 July 2018
0197-0186/

deficiency, all had neonatal onset, severe epileptic encephalopathy (Haberle et al., 2012; Spodenkiewicz et al., 2016).

The exact role of Glul in epilepsy, however, has been difficult to establish, and the mechanism by which Glul deficiency might cause disease is poorly understood. First, MTLE patients with secondary Glul deficiency may suffer from the consequences of the Glul deficiency as well as from effects of the primary insult (which is unknown in most cases). Second, the patients with congenital (primary) Glul deficiency were not only suffering from the cerebral consequences of Glul insufficiency, but also from the consequences of multiple organ failure with secondary effects on the brain (Spodenkiewicz et al., 2016). Third, methionine sulfoximine has several effects other than inhibiting Glul. It decreases tissue glutathione (Shaw and Bains, 2002), increases astrocyte glycogen (Bernard-Helary et al., 2002) and excites neurons via a Glul-independent mechanism (Kam and Nicoll, 2007). To separate the consequences of a primary Glul defect in the CNS from those of other events, a genetic approach is urgently needed; however, attempts to resolve this issue have been met with limited success. Mice completely deficient in Glul die already at embryonic day E3 (He et al., 2007) and mice with deficiency limited to the CNS die three days after birth (He et al., 2010).

Because cortical structures are important for seizure generation and propagation (Eid et al., 2008; Blumenfeld et al., 2009) and because intact brain stem functions are required for survival, we selectively deleted Glul in the cerebral cortex (i.e. neocortex and hippocampus) of mice by taking advantage of the Emx1-IRES Cre line, which directs Cre-mediated gene deletion in the cortex while sparing critical brain stem regions (Gorski et al., 2002). Using this approach, we demonstrate here that loss of cortical Glul causes abnormal glutamate signaling and induces astrogliosis and vascular impairment, ultimately culminating in spontaneous recurrent (epileptic) seizures and neuron loss.

2. Materials and methods

2.1. Materials

N,N′-Methylenebisacrylamide was from Promega (Madison, WI, USA). Molecular mass markers for SDS polyacrylamide gel electrophoresis (SDS PAGE) and nitrocellulose sheets (0.22 μm pores, 100% nitrocellulose) were from GE Healthcare (Buckinghamshire, UK). Paraformaldehyde was from Electron Microscopy Sciences (Hatfield, PA, USA), and glutaraldehyde was from TAAB (Reading, UK). Sodium dodecyl sulfate (SDS) of high purity (> 99% C12 alkyl sulfate) was from Millipore (Carrigtwohill, C. Cork, Ireland). Electrophoresis equipment was from Hoefer Scientific Instruments (San Francisco, CA, USA). Permount mounting medium, ProLong anti-fade DAPI media, DyNAzyme II DNA Polymerase were from ThermoFisher Scientific (Waltham, Massachusetts, USA). All other reagents were obtained from Sigma-Aldrich (St. Louis, MO, USA).

2.2. Animals

All animal studies were carried out in accordance with the European Communities Council Directive of 24 November 1986 (86/609/EEC) and the United States Animal Welfare Act. Formal approval to conduct the experiments was obtained from the animal subjects review board of the Norwegian Governmental Institute of Public Health (Oslo, Norway) and the Institutional Animal Care and Use Committee at the Yale School of Medicine. Care was taken to avoid suffering and minimize the number of the experimental animals. The mice were housed in individually ventilated (IVC) cages at constant temperature (22 ± 0.7 °C) and humidity (56 ± 6%), and were fed with Harlan Teklad 2018 (Harlan Laboratories Inc., Indianapolis, IN, USA) with the access to water *ad libitum*. Biopsies from ear or tail were collected for determining genotype.

As Fig. 1A shows, to generate the conditional Glul KO mouse line ($Glul^{f/f}$), the targeting vector was prepared by recombineering as described by Lee and co-workers (Lee et al., 2001). Briefly, approximately 12 kb of Glul genomic fragment containing the entire Glul was retrieved from the bacterial artificial chromosome (BAC) clone, RP24-326N10 (obtained from the BACPAC Resources Center at the Children's Hospital Oakland Research Institute, Oakland, CA) by gap repair. The 5′LoxP site was inserted in intron 1 at position 628, nucleotides 5′ of exon 2, and the second 3′LoxP sequence together with the Frt-PGKneo-Frt selectable marker was inserted 140 nucleotides 5′ of exon 7. Thus, loxP sites were inserted on each flank of the DNA encoding exon 2–6. This vector containing approximately 4 kb and 2.9 kb of 5′-long and 3′-short arms, respectively, was then linearized by NotI digestion, purified and then electroporated into ES cells, which was derived from F1(129sv/C57BL6j) blastocyst. ES cells were cultured in the presence of G418 and Ganciclovir after electroporation according to Wurst and Joyner (1999) and drug resistant colonies were picked and cultured in 96-well plates. Drug resistant ES clones were screened by nested long-range PCR using primers specific to genomic sequences outside the homology arms and LoxP sites to identify targeted ES clones. Targeted clones were expanded and screened again to confirm their identity prior to the generation of chimeric animals by aggregation with CD1 morula. Chimeric males were then bred with ROSA26-Flpe female (Soriano, 1997) to remove the PGKneo cassette to generate the final Glul floxed allele. Two chimeric founder lines (1F7 and 1B4) were produced, and backcrossed more than ten generations into the C57BL/6 background. Both were crossed with Cre-lines as described. The Flox-Glul mice were first tested by crossing with a general deletor strain (Htrp1-Cre: Jackson Laboratories, Stock No. 004302; RRID: IMSR_JAX:004302) mediating deletion in all cells including germ cells and a global astrocyte deletor (hGFAP-Cre: Jackson Laboratories, Stock No. 004600; RRID: IMSR_JAX:004600). Heterozygote Glul mice of two lines were obtained and they were fertile, but homozygote knockout mice were not obtained (data not shown) in agreement with data from others using another Flox-Glul mouse line (He et al., 2007, 2010). We then tested the Emx1-IRES-Cre line (Jackson Laboratories, Stock No. 005628; Gorski et al., 2002; RRID: IMSR_JAX:005628) by crossing it with a reporter line [$Gt(ROSA)26Sor^{tm4(ACTB-tdTomato,-EGFP)Luo}$; Jackson Laboratories, Stock No. 007676; RRID: IMSR_JAX: 007676). The resultant litters had Cre expressed in neurons, astrocytes and oligodendrocytes (data not shown) consistent with data from others (Gorski et al., 2002). Crossing the female or male Emx1-IRES-Cre line with the male or female Flox-Glul mice resulted in live mice lacking Glul in the cerebral cortex (Fig. 1B). The breeding scheme to generate cortical Glul knockouts was as follows:

1st generation: heterozygote Cre-mice ([$Emx1\text{-}Cre^{+/0}$]) were crossed with homozygote Flox-Glul mice ([$Glul^{f/f}$]). This crossing gave two possible genotype combinations, namely [$Emx1\text{-}Cre^{+/0}$;$Glul^{f/w}$] and [$Glul^{f/w}$].

2nd generation: the [$Emx1\text{-}Cre^{+/0}$;$Glul^{f/w}$] mice were crossed with homozygote Flox-Glul mice ([$Glul^{f/f}$]). This crossing gave four possible genotype combinations: [$Emx1\text{-}Cre^{+/0}$;$Glul^{f/f}$], [$Emx1\text{-}Cre^{+/0}$;$Glul^{f/w}$], [$Glul^{f/f}$] and [$Glul^{f/w}$].

The [$Emx1\text{-}Cre^{+/0}$;$Glul^{f/f}$] mice are hereafter referred to as cortical knockouts (cKO), while the [$Emx1\text{-}Cre^{+/0}$;$Glul^{f/w}$] are referred to as conditional heterozygotes and the mice lacking Cre ([$Glul^{f/f}$] and [$Glul^{f/w}$]) are referred to as wildtype (WT).

The phenotypes of the two Flox-Glul founder lines were similar (data not shown). Most of our study here was based on the knockout generated from the 1F7 founder line.

2.3. Genotyping

Biopsies were digested (95 °C, 1 h) with alkaline lysis solution (25 mM NaOH and 0.2 mM EDTA) and chilled on ice before addition of

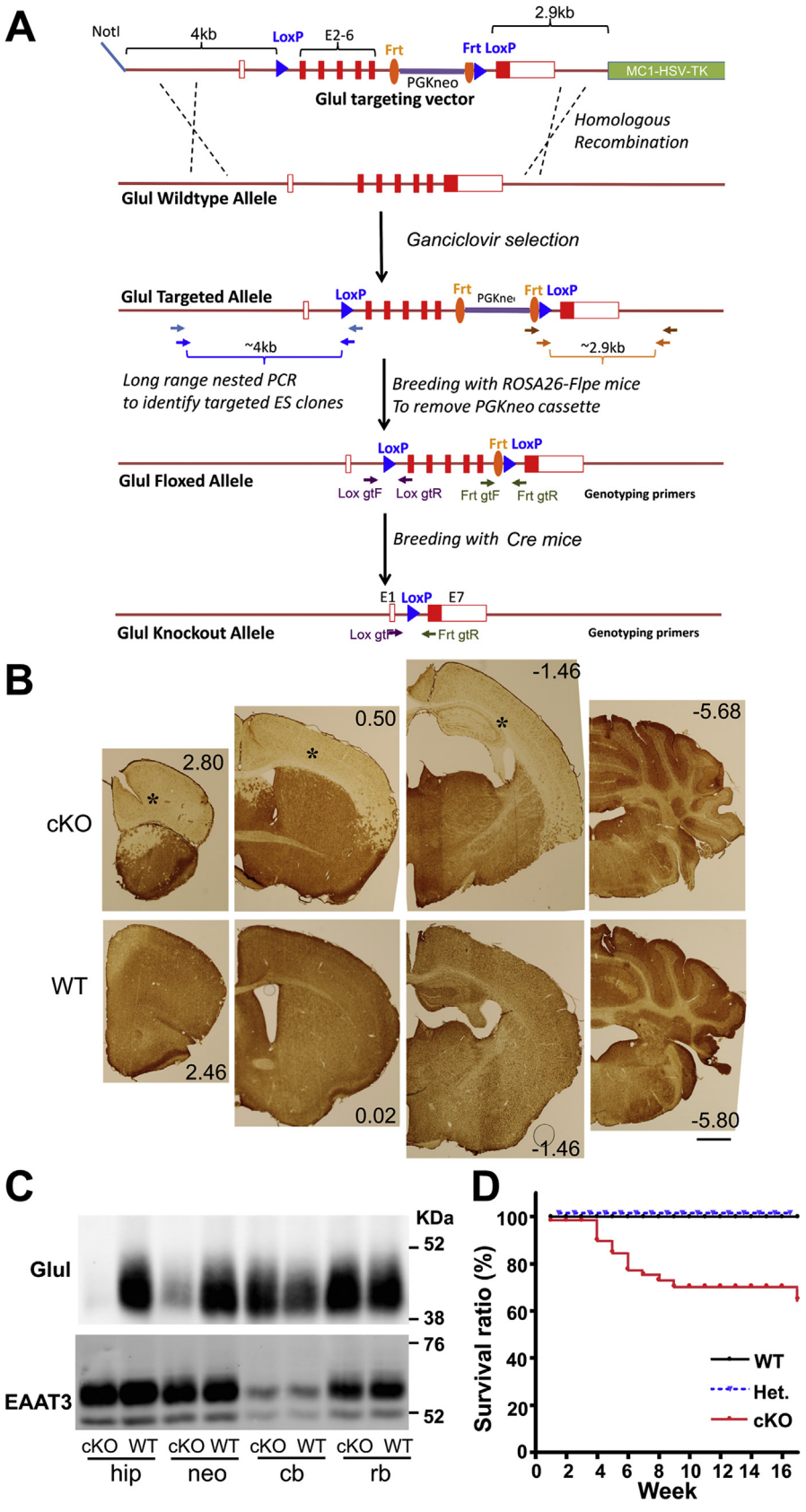

Fig. 1. Selective deletion of the Glul gene in the cerebral cortex was achieved by crossing Emx1-Cre mice with Glul-flox mice. (**A**) Construction of Glul-flox mice (see Methods for details). (**B**) The resulting Glul conditional knockout mice (cKO) lacked Glul protein in the neocortex and the hippocampus. Sections through different parts of brains from cKO and wild-type (WT) mice were labeled with antibodies to Glul. Note that there is hardly any staining in the cerebral cortex (*) of the cKO mice. And as the Emx1-Cre driver is not active in the cerebellum, Glul expression is preserved. Scale bar 1 mm. (**C**) Immunoblots confirmed that Glul labeling was virtually absent in the hippocampus and neocortex of the cKO mice. Identical blots were prepared from fresh brain tissue from the hippocampus (hip), neocortex (neo), cerebellum (cb) and rest of the brain (rb) from cKO and WT mice, and probed with antibodies to Glul or EAAT3 as indicated. (**D**) Mortality of the cKOs during 16-week-observation period (n = 97 mice). Note that the mortality was highest between 4 weeks and 9 weeks with few deaths before and after.

neutralizing solution (40 mM Tris-HCl). The primers to detect the GS-flox genotype were GS lox gtF (5′-agtcagcagtgtgctccttg-3′) and GS lox gtR (5′-gctcagctcttggaacaacc-3′). The cycle is described as following: 1.94 °C 3 min; 2.94 °C 30 s; 3.55 °C 30 s; 4.72 °C 30 s; Repeat 2–4 for 35 cycles; 5.72 °C, 4 min. The expected PCR products were 346 bp for the wild-type allele and 440 bp for the flox allele. The primers to detect the Emx1-Cre (Gorski et al., 2002) are oIMR1084 (5′-GCG GTC TGG CAG TAA AAA CTA TC-3′) and oIMR1085 (5′-GTG AAA CAG CAT TGC TGT

CAC TT-3′). The cycle is described as following: 1.94 °C 3 min; 2.94 °C 30 s; 3.51.7 °C 1 min; 4.72 °C 1 min; Repeat 2–4 for 35 cycles; 5.72 °C, 2 min. The expected PCR product was about 100 bp (data not shown).

2.4. Antibodies

Affinity purified anti-peptide antibodies to sheep anti-EAAT2 (GLT-1; Ab#8; Li et al., 2012; RRID: AB_2714090), rabbit anti-EAAT1 (GLAST; Ab#314; Holmseth et al., 2009; RRID: AB_2314561) and rabbit anti-EAAT3 (EAAC1; Ab#371 Holmseth et al., 2012a; RRID: AB_2714048) were from the same batch as previously described. Because antibody batches may differ from each other (Danbolt et al., 2016a), we identify antibody batches by the unique identification number ("Ab#") they are given by our electronic laboratory information system (software provided by Science Linker AS; Oslo, Norway).

Rabbit anti-VGLUT1 (Cat. No. 135303; RRID: AB_887875) was a gift from Henrik Martens (Synaptic System GmbH, Goettingen, Germany). Rabbit anti-GLUT1 (Cat. no. ab14683; RRID: AB_301408) were from Abcam. Rabbit anti-glutamine synthetase (Cat. no G2781; RRID: AB_259853), and mouse monoclonal anti-GFAP (Cat no. G3893; RRID: AB_477010) were from Sigma (St. Louis, MO, USA). IRDye 680RD Donkey anti-Rabbit IgG (H + L) (Cat. no. P/N 926–68073; RRID: AB_10954442) and IRDye 800CW Donkey anti-mouse IgG (H + L) (Cat. no. P/N 926–32212; RRID: AB_621847) were from Li-Cor Bioscience UK Ltd, and Alexa Fluor 680 AffiniPure Donkey anti-sheep IgG (H + L) (Cat. no. 713-625-147; RRID: AB_2340753) was from Jackson ImmunoResearch. Alexa fluor goat anti-mouse 488 (Cat. no A11029; RRID: AB_2534088), goat anti-rat 488 (Cat. no A11006; RRID: AB_2534074), goat anti-rabbit 555 (Cat. no A21429; RRID: AB_2535850) antibodies were purchased from Molecular probes (Eugene, OR, USA).

2.5. Tissue preparation for electrophoresis and immunoblotting

The tissue wet weight was recorded before the tissue was homogenized in 10–20 vol of 1% SDS in 10 mM sodium phosphate buffer (NaPi) with pH 7.4 (NaPi). As brain tissue contains close to 10% protein (Lowry, 1953; Lowry et al., 1954), the wet weight gave a first approximation of the protein content. The total protein concentrations of the extracts were subsequently determined by Lowry assay (Lowry et al., 1951), and then diluted to the same concentrations in SDS-sample buffer (Laemmli, 1970), and loaded onto SDS-polyacrylamide gel (Laemmli, 1970) using Hamilton syringes (Hamilton Robotics, NV, USA) to ensure correct loading. After electrophoresis and immunoblotting, Ponceau-S stain or total REVERT protein staining (Li-Cor, Lincoln, NE, USA) of the membranes in combination with Coomassie blue stain of the gels were used to check that the blots indeed had received equal amounts of protein after transfer. Identical blots were prepared in parallel and probed with different primary antibodies. Because the expression of housekeeping proteins can alter in diseased state (Ferguson et al., 2005) and glutamine synthetase deficiency in murine cortex causes progressive neurodegeneration, house keeping proteins might not be optimal as useful references in the present study, and were only used when stated.

Briefly, the blots were first rinsed in PBS (10 mM NaPi pH7.4 and 135 mM NaCl) and then were blocked (1 h) with 0.05% (w/v) casein in PBS before incubating with primary antibodies in bovine serum albumin (BSA; 30 mg/ml) in PBST (PBS with 1 ml/L Tween 20 and 0.5 mg/ml NaN_3) overnight, room temperature. The membrane was rinsed (4 × 10 min) with PBST before incubation (1 h) in secondary antibody solution (1:20000). Rinse membrane several times with PBST and then PBS to remove residual Tween 20 before scanning. The blots were examined for immunofluorescence using an infrared scanner (Licor Odyssey system, LI-COR Biotechnology-UK Ltd, Cambridge, UK). Densitometric data were extracted from the images using the Gel analyzer tool included in our electronic laboratory information system (software provided by Science Linker AS; Oslo, Norway). The results are presented as percent of control (average ± SEM where n represents the number of pairs of littermates). Unpaired student's T-test was used to compare the means of two groups of data. P-values are given when there were statistically significant differences ($p < 0.05$) between the data from the Emx1-Glul knockout mice and the control mice.

2.6. Immunocytochemistry

Mice were transcardially perfused with 4% formaldehyde in 0.1 M NaPi with or without 0.05% glutaraldehyde (Danbolt et al., 1998). Briefly, they were deeply anesthetized by intraperitoneal injection with ZFR cocktail (at least 0.1 ml per 10 g body weight). ZRF is of a mixture of zolazepam (3.3 mg/ml; CAS 31352-82-6), tiletamine (3.3 mg/ml; CAS 14176-49-9), xylazine (0.5 mg/ml; CAS 7361-61-7) and Fentanyl (2.6 μg/ml; CAS 437-38-7). After cessation of all reflexes, the mice were perfused first with 0.1 M NaPi pH7.4 to wash out blood and then immediately followed by 4% formaldehyde in 0.1 M NaPi with or without 0.05% glutaraldehyde, as stated, for 5 min. The relevant tissues were collected and immersed in fixative for about 2–4 h at room temperature. Sections (40 μm thick) were cut from the fixed unfrozen tissue using a Vibratome 1000 plus® (Vibratome, Bannockburn, UK).

Diaminobenzidine-peroxidase labeling was performed as described (Lehre et al., 1995). Briefly, the sections were pre-incubated in 1% hydrogen peroxide in 0.1 M NaPi, rinsed and treated (30 min, room temperature) in 1 M ethanolamine in 0.1 M NaPi with 0.5% (v/v) Triton X-100 and rinsed (x 3) in PBS (0.135 M NaCl, 10 mM NaPi pH 7.4 with 0.5% (v/v) Triton X-100) prior to incubation (1 h, room temperature) in blocking solution (10% (v/v) newborn calf serum (NCS) in TBST (TBS with 0.5% (v/v) Triton X-100), with 0.1 mg/mL NaN_3). Next, sections were incubated (over night, room temperature) with primary antibodies diluted (at concentrations as stated) in blocking solution. After rinsing (x 5) in TBST with 1% (v/v) NCS, the sections were incubated (1 h, room temperature) with secondary antibodies diluted (1:300) in TBST with 1% (v/v) NCS, and, after rinsed as above, incubated (1 h, room temperature) with streptavidin-biotinylated horseradish peroxidase complex, diluted (1:300) in TBST with 1% (v/v) NCS. The rinsing steps were repeated and sections were then rinsed (x3) in PBS prior to the color development step with diaminobenzidine-peroxidase.

Immunofluorescent labeling was done as previously described (Zhou et al., 2012). Briefly, The sections were rinsed (3 × 5 min) in TBST (TBS with 0.5% Triton X-100), treated with 1 M ethanolamine in 0.1 M NaPi pH 7.4 for 30 min, washed in TBST, incubated (1 h) in TBST containing 10% newborn calf serum and 3% bovine serum albumin followed by incubation with primary antibodies and finally with secondary antibodies (Alexa fluor goat anti-mouse 488, Molecular probes; Eugene, OR, USA) diluted 1:1000 dilution. After being washed 3 times with TBST, the sections were then mounted with ProLong Gold antiFade mounting medium with DAPI (ThermoFisher Cat. No. P36935, Waltham, MA, USA) or Fluoroshield with DAPI histology mounting medium (Sigma, F6057) and examined using a Zeiss Axioplan 2 microscope equipped with a Zeiss LSM 510 meta confocal scanner head (Zeiss, Jena, Germany).

2.7. Histological staining

2.7.1. Nissl staining

Sections were mounted onto SuperFrost Plus slides (ThermoFisher, Waltham, MA, USA), air dried and incubated (3 min) in Walter's cresyl violet solution on a heating plate. Excess staining solution was removed, the stain was differentiated in tap water (3 min) and the sections were dehydrated in graded ethanol, cleared in xylene and mounted with Permount (Cat. no: 12377369, Fisher Scientific).

2.7.2. NeuroSilver staining

Vibratome sections were stained using the FD NeuroSilver kit according to the manufacturer's instructions (FD NeuroTechnolologies

Inc, Columbia, USA). Briefly, sections were rinsed in MilliQ water (2 × 5 min), transferred into a mixture containing equal volumes of Solution A and B (2 × 10 min) and incubated in a mixture of equal volumes of Solution A and B with Solution E, and then in a mixture of Solution C and Solution F (2 × 2 min). After incubation in a mixture of Solution D and Solution F for 5 min, the sections were rinsed in MilliQ water (2 × 3 min) and incubated in Solution G (2 × 5 min). The sections were finally mounted on SuperFrost slides, air dried, cleared in xylene and coverslipped with Permount.

2.8. Amino acid measurements

Mice were decapitated, and the heads immediately plunged into liquid nitrogen for 5 s. The neocortex and hippocampi were dissected out on ice, weighed, and homogenized in 10 vol of perchloric acid, 2% (vol/vol) containing α-amino adipate, 1 mmol/L. Protein was removed by centrifugation, and the supernatant was neutralized with KOH, 10 mol/L. Amino acids were quantified by HPLC and fluorescence detection after pre-column derivatization with o-phthaldialdehyde, as described (Dahlberg et al., 2014).

2.9. EEG

Mice were anesthetized with 0.25–2% isoflurane (Baxter, Deerfield, Ill.) in O_2, placed in a stereotaxic frame (David Kopf Instruments, Tujunga, CA, USA) and implanted with stainless-steel screw electrodes (Plastics One, Roanoke, Va, USA) that were positioned in the epidural space, over the parietal cortex bilaterally. The female ends of the electrodes were inserted in a pedestal (Plastics One, Roanoke, VA; USA) which was cemented onto the skull with UV light cured acrylated urethane adhesive (Loctite 3106 Light Cure Adhesive, Henkel Corp., Rocky Hill, CT, USA) to form a headcap. The mice were placed individually in custom-made Plexiglas cages. A 6-channel cable was connected to the electrode pedestal on one end and to a commutator (Plastics One) on the other. A second cable connected the commutator to the digital EEG recording unit (CEEGraph Vision LTM, Natus/Bio-Logic Systems Corp., San Carlos, CA, USA). Digital cameras with infrared light detection capability were used to record animal behavior (two cages per camera). The digital video signal was encoded and synchronized to the digital EEG signals. Seizures were identified by visual inspection of the EEG record. The Racine criteria (Racine et al., 1973) were modified and used to classify the seizures from the video records, as follows: Stage 1, immobilization, eye blinking, twitching of vibrissae, and mouth movements; Stage 2, head nodding, often accompanied by severe facial clonus; Stage 3, forelimb clonus; Stage 4, rearing, Stage 5, rearing, falling, and generalized convulsions.

2.10. fMRI imaging and data analysis

For imaging experiments, animals were first anesthetized using 3% isoflurane in a mixture of O_2 and N_2O (30/70%), then placed in a custom built frame where they were freely breathing through a nose cone. During the scanning procedure, isoflurane was turned off and anesthesia was maintained using a subcutaneous infusion of dexmedetomidine (Zoetis): 2 μL + 4 μL/h per gram of body weight, at 0.05 mg/mL concentration. Body temperature was monitored using a rectal probe, and maintained within 35–37 °C using warm water pumped through the bed.

MRI data were obtained on a modified 9.4T system with Varian spectrometer and custom built 1H 12 mm surface coil. Images were acquired over 8 contiguous coronal slices (thickness = 1 mm), covering the parenchyma between the olfactory bulb and cerebellum, with an in-plane field of view of 1.28 × 1.28 cm. Resting-state (task-free) images were obtained using an echoplanar imaging (EPI) sequence (TR/TE = 1000/13 ms in a 32 × 32 matrix, for an in-plane resolution of 250 μm) for 6 min (360 repetitions), and repeated three times per animal. The cerebrovascular reactivity (CVR; repeated twice per animal) functional scans lasted for 9 min with 10% CO_2 added to the breathing gas mixture between minutes 3 and 6 of the acquisition. Lastly, a high-resolution spin-echo anatomical image (32 slices at 0.25 mm thickness, 128 × 128 for an in-plane resolution of 100 μm, 4 averages) was used for co-registration and volumetric analysis.

Using AFNI (https://afni.nimh.nih.gov/), functional images of CO_2 challenge were corrected for motion and spatially smoothed using a Gaussian filter (FWHM = 1 mm). Parametric maps of CVR were generated from a voxel-level linear model and expressed as the t-statistical value of the contrast between baseline (Frames 1 to 180) and CO_2 challenge (Frames 210 to 360).

Anatomical images were used to generate a non-linear transform from each animal subject's native space to a common standard space. The transform was then applied to all parametric maps of CVR, which were then Fisher transformed. Group averages and contrasts were calculated with a voxel-level linear model for each modality with an adjusted threshold of $p < 0.05$ corrected for multiple comparisons. Finally, brain volume was estimated by manually drawing an intracranial mask over the anatomical images (in native space) by an experimenter blinded to group conditions.

2.11. Open field test (OF)

The 15-min OF tests were carried out using 4–15 weeks old (male and female) under a light intensity of 100 ± 10 Lux. The tests were performed between 4.0 and 0.5 h before the start of dark cycle. First, animals were placed in the testing room in their home cage for at least 10 min to acclimate. The test started by gently removing each mouse from their home cage and immediately placing them in the center of the test chamber (chamber dimensions: L50 x W50 x H21.5 cm). A series of 12.5 × 12.5 cm zones were defined in the test chamber. The outer zone consists of 12 blocks while the center/inner zone consists of 4 blocks. The entire session was videotaped for later analysis. All the animals were first-time for OFs. After the tests, the animals were housed in a new cage, and the number of feces produced during the sessions was counted. 70% ethanol was used to clean the chamber between sessions. All OF videos were then analyzed by one individual in a double-blind manner. Horizontal activities were measured by total number of crossings (during each min and in 15 min) and vertical activities were measured by the total number of rearing (to the walls). For accessing anxiety behavior, both total number of crossings to the center and the number of fecal boli produced were counted.

2.12. Experimental design and statistical analysis

All experiments were performed at least three times unless stated otherwise. Statistical significance between two independent samples was assessed by Student's *t*-test. Statistical analyses and plotting graphs were performed with GraphPad Prism4 (GraphPad Software). Differences between groups were judged to be significant when P values were smaller than 0.05. *, ** and not significant represent $P < 0.05$, $P < 0.01$ and not significant, respectively. Error bars always indicate the standard error of the mean (± SEM) except when stated (Table 1). No samples or animals were excluded from the analysis. For HPLC analysis, data were obtained in a blind manner in which the experimenters did not know the mouse genotypes.

3. Results

3.1. Mice with cortical deletion of Glul are viable

Our model of cortical Glul deficiency was created by first tagging the Glul gene with flanking LoxP sites to permit cyclization recombinase (Cre)-mediated deletion of exons 2–6 (Fig. 1A). These animals are hereafter referred to as Glul-flox mice. We then crossed the

Table 1
Total amino acids in the cerebral cortex (including hippocampus) from cortical Glul knockouts and wildtype littermates.

	Cortex		Cerebellum	
	WT (Cre^{-}; $GS^{f/?}$)	cKO (Cre^{+}; $GS^{f/f}$)	WT (Cre^{-}; $GS^{f/?}$)	cKO (Cre^{+}; $GS^{f/f}$)
Asp	2.86 ± 0.52	0.86 ± 0.19*	2.24 ± 0.36	2.38 ± 0.31
Glu	9.45 ± 1.76	4.82 ± 0.52*	8.17 ± 0.33	8.58 ± 0.59
Gln	4.39 ± 0.24	1.05 ± 0.25*	4.81 ± 0.30	4.90 ± 1.17
Tau	10.20 ± 2.87	12.43 ± 0.89	6.09 ± 0.13	7.46 ± 0.79
Ala	0.84 ± 0.16	0.93 ± 0.10	0.25 ± 0.17	0.30 ± 0.12
GABA	1.55 ± 0.48	0.82 ± 0.18*	1.08 ± 0.36	1.08 ± 0.03

Amino acid concentrations (nmol per mg wet weight of whole tissue) were determined by means of HPLC in samples from three conditional Glul cortical knockouts (cKO) and two wildtype littermates. The mice, all females, were about 8 weeks old. The cortex samples comprised the entire neocortex and hippocampus. The numbers represent mean ± SD.

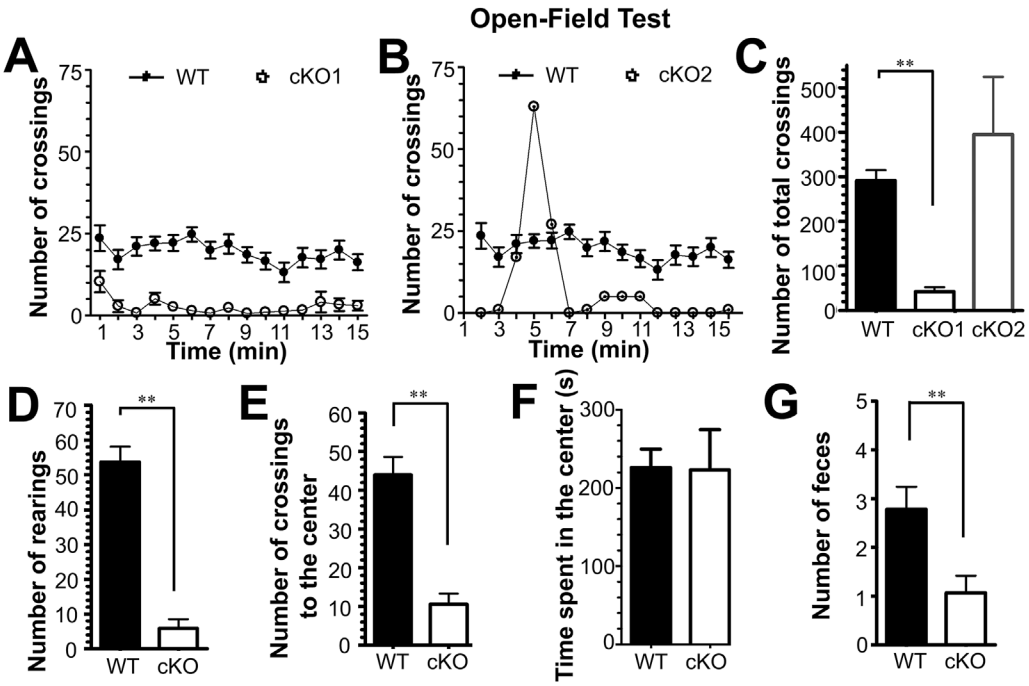

Fig. 2. Glul conditional knockout (cKO) mice exhibited altered locomotive activities when subjected to the 15-min open-field test. A total of 15 pairs of WT and cKO mice (21–103 days old) were tested (10 pairs of males and 5 pairs of females). (**A**) Most of the cKO mice (cKO1; 9 pairs) were clearly hypoactive during the entire test period. (**B**) The remainder (cKO2; 6 pairs) had one or more sudden bursts of activity during the test period. The number of total crossings of all groups of cKO1 and cKO2 were represented in Panel (**C**). (**D**) The cKO mice were less active vertically (lower number of rearings), (**E**) they had fewer entries to the center, (**F**) but spent comparable time in the center. (**G**) The cKO also produced a lower number of feces during the test session. **p < 0.01.

Glul-flox mice with Emx1-IRES-Cre mice, in which Cre-expression is primarily restricted to telencephalic regions, in particular parts that give rise to the neocortex and hippocampus (Gorski et al., 2002).

Breeding of our Glul-flox mice with the Emx1-Cre mice resulted in conditional knockout (cKO) mice where the Glul protein was abolished in most of the neocortex and hippocampus (Fig. 1BC). Because Glul is predominantly an astroglial enzyme, it seems reasonable to assume that the Emx1-Cre driven deletion mostly affects astrocyte function. The glutamate transporters EAAT3 (Fig. 1C) and EAAT2 (data not shown) were still present in the affected area, as these genes had not been floxed and therefore could not be excised by Cre. The cortical expression levels of Glul protein in heterozygous mice were approximately half of those in wild-type (WT) mice (52%, n = 2 pairs of mice). Further, we observed that Glul protein was absent from the cKO cortex at birth (data not shown), consistent with the reported start of Cre-expression at E10.5 (Gorski et al., 2002). Genotyping at 3 weeks of age from a breeding scheme ($Cre^{+/0}$; $Glul^{f/w}$ x $Cre^{0/0}$; $Glul^{f/f}$) revealed a typical Mendelian distribution (2WT: 1Het: 1cKO) of 47.8% wild-type (WT; $Cre^{0/0}$; $Glul^{f/f\ or\ f/wt}$; n = 199), ~27.2% heterozygous ($Cre^{+/0}$;$Glul^{f/w}$; n = 113) and ~25.0% cKO mice ($Cre^{+/0}$; $Glul^{f/f}$; n = 104). Thus, the deletion did not appear to increase prenatal mortality. Increased mortality was first noted after three weeks (Fig. 1D).

3.2. Cortical deletion of Glul results in late-onset epileptic seizures

Despite deletion of Glul before birth, neither heterozygous nor homozygous cKO mice could be distinguished from their WT littermates with respect to overall appearance during the first two postnatal weeks. At postnatal week 3, the cKO mice began to exhibit behavioral abnormalities such as hypoactivity and periodic running fits when subjected to mild stimulation such as removing the cage lid or gentle knocking on the cage. To further assess the behavioral phenotype, we subjected the mice to the open field test which measures general locomotive activities. The mice (4–15 weeks old cKO and WT littermates) were observed for 15 min each. This was sufficient to reveal alterations in the locomotive activities (Fig. 2). One subgroup of the cKO mice (cKO1, 9 pairs of WT and cKO) were almost inactive during the test (Fig. 2AC) while another subset (cKO2, 6 pairs) showed hypoactivity interrupted by bursts of sudden wild running (Fig. 2BC). The cKO mice exhibited reduced vertical activity (Fig. 2D) and fewer entries to the center of the chamber (Fig. 2E), while the time spent in the center by the cKO mice was comparable to that of WT littermates (Fig. 2F). During these sessions, fewer fecal boli were produced by the cKO mice, suggestive of reduced anxiety (Fig. 2G).

Besides periodic running fits, facial automatisms with occasional falling and forelimb clonus were observed in the cKO mice older than 6 weeks, suggestive of seizures. Continuous video-intracranial EEG

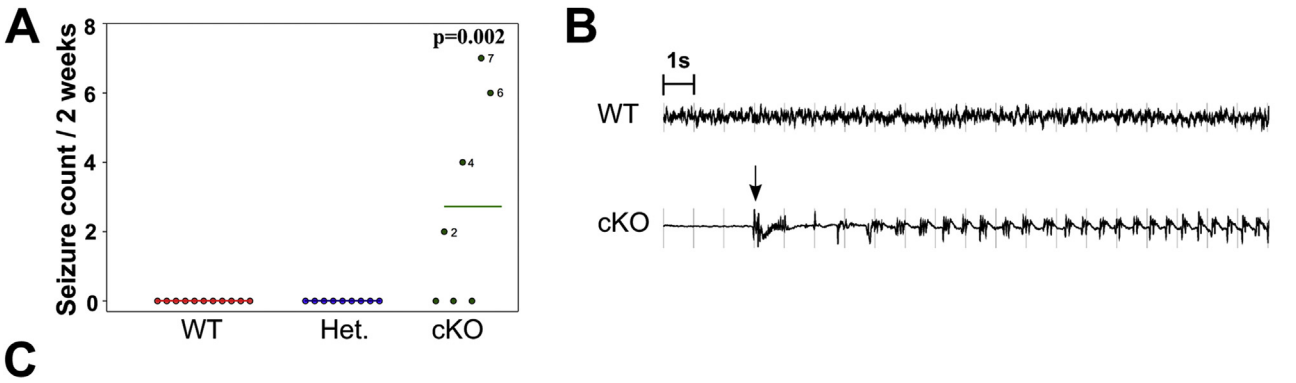

C

				Days of EEG Analysis														
Mouse ID	Age (days)	Genotype	Sex	1	2	3	4	5	6	7	8	9	10	11	12	13	14	Total Seizures
1.5M5	33	WT	M	0	0	0	0	0	0	0	0	0	0	0	0	0	0	0
4.3M3	38	WT	M	0	0	0	0	0	0	0	0	0	0	0	0	0	0	0
4.3M4	38	WT	M	0	0	0	0	0	0	0	0	0	0	0	0	0	0	0
4.3F1	38	WT	F	0	0	0	0	0	0	0	0	0	0	0	0	0	0	0
3.4M2	40	WT	M	0	0	0	0	0	0	0	0	0	0	0	0	0	0	0
3.4F3	40	WT	F	0	0	0	0	0	0	0	0	0	0	0	0	0	0	0
4.1F3	86	WT	F	0	0	0	0	0	0	0	0	0	0	0	0	0	0	0
4.6F1	152	WT	F	0	0	0	0	0	0	0	0	0	0	0	0	0	0	0
2.4F1	152	WT	F	0	0	0	0	0	0	0	0	0	0	0	0	0	0	0
1.4M2	166	WT	M	0	0	0	0	0	0	0	0	0	0	0	0	0	0	0
2.3M4	208	WT	M	0	0	0	0	0	0	0	0	0	0	0	0	0	0	0
3.4M3	40	Het	M	0	0	0	0	0	0	0	0	0	0	0	0	0	0	0
3.4F2	40	Het	F	0	0	0	0	0	0	0	0	0	0	0	0	0	0	0
8.3 M1	40	Het	M	0	0	0	0	0	0	0	0	0	0	0	0	0	0	0
9.2 M1	43	Het	M	0	0	0	0	0	0	0	0	0	0	0	0	0	0	0
9.2 M2	43	Het	M	0	0	0	0	0	0	0	0	0	0	0	0	0	0	0
9.2M3	43	Het	M	0	0	0	0	0	0	0	0	0	0	0	0	0	0	0
6.2M10	69	Het	M	0	0	0	0	0	0	0	0	0	0	0	0	0	0	0
9.3F2	93	Het	F	0	0	0	0	0	0	0	0	0	0	0	0	0	0	0
2.3M1	208	Het	M	0	0	0	0	0	0	0	0	0	0	0	0	0	0	0
1.5M1	33	cKO	M	0	0	0	0	0	0	0	0	0	0	0	0	0	0	0
1.5M3	33	cKO	M	0	0	0	0	0	0	0	1	0	0	0	1	0	0	0,2
3.4M1	38	cKO	M	0	0													0
8.3M4	38	cKO	M	0	0	0	0											0
11.4F2	61	cKO	F	0	0	0	0	0	0	0	0	0	0	0	0	0	0	0
11.4F6	61	cKO	F	0	0													0
8.5M1	69	cKO	M	0	0	0	0	0	0	0	0	0	0	1	1,1	1	0	3,1
8.5M6	69	cKO	M	0	0	0	0	0	0	0	0	0	0	0	0	0	0	0
6.2M2	69	cKO	M	2	1	10,5	4,2											16,8
6.2M6	69	cKO	M	0	0													0
6.2M7	69	cKO	M	2	0	43,7	41,3											84,12
6.2F3	69	cKO	F	0	0													0
4.1F2	86	cKO	F	3	0	0	0	1	0	0	0	0	0	1	1,1	0	0	4,3
2.4F2	152	cKO	F	0	0	0	0	4	0	0	0	0	0	0	1	0	1	0,6

Fig. 3. (**A**) The bars indicate the average number of seizures from the animals in **C** after exclusion of the 7 cKO that died during recordings. No seizures were observed in the wildtype (WT) or heterozygous Glul knockout (Het) mice, whereas the cKO mice had an average of 2.71 ± 1.13 seizures during the 2-week period ($p = 0.002$). Twelve of 19 (63.2%) seizures were severe (Racine Grade 4–5). (**B**) Representative EEG tracing of a WT mouse and a cKO mouse are shown. The arrow indicates the start of the seizure. The severity of the seizure was not apparent by EEG, and examination of the concurrent video record was necessary for severity staging. (**C**) Daily seizure counts and severity assessments over a 14-day recording period. Wildtype (WT; n = 11: 6 males, 5 females), heterozygous Glul knockout (Het; n = 9: 7 males, 2 females), and homozygous Glul knockout (cKO; n = 14: 9 males, 5 females) mice were monitored by continuous video-intracranial EEG analysis for two-weeks. The number of seizures per day is provided. Mild (Racine Grade 1–3) and severe (Racine Grade 4–5) seizures are indicated by blue and red numbers respectively. Seven of the 14 cKO animals died at different time points during the recording (indicated by dark gray shading). These animals are excluded from the plots in **A**. Abbreviations: F, female; M, male.

recordings of mice aged 4–28 weeks demonstrated spontaneous recurrent seizures in 4 of 7 cKO mice, but not in any of the heterozygous (n = 9) or in the WT (n = 11) mice (Fig. 3). The frequency, duration and behavioral severity of the seizures varied among animals, with a tendency for the seizures to become more frequent as the animals aged.

3.3. Cortical deletion of Glul causes progressive neurodegeneration and ultimately hippocampal sclerosis

Examination of Nissl-stained brain sections from 6 weeks old Glul cKO mice did not reveal any major abnormalities in the neocortical and hippocampal cytoarchitecture. However, focal lesions (small islands of neuronal loss) in the neocortex were occasionally found at this age, but only in some of the mice (data not shown). As the mice aged, more

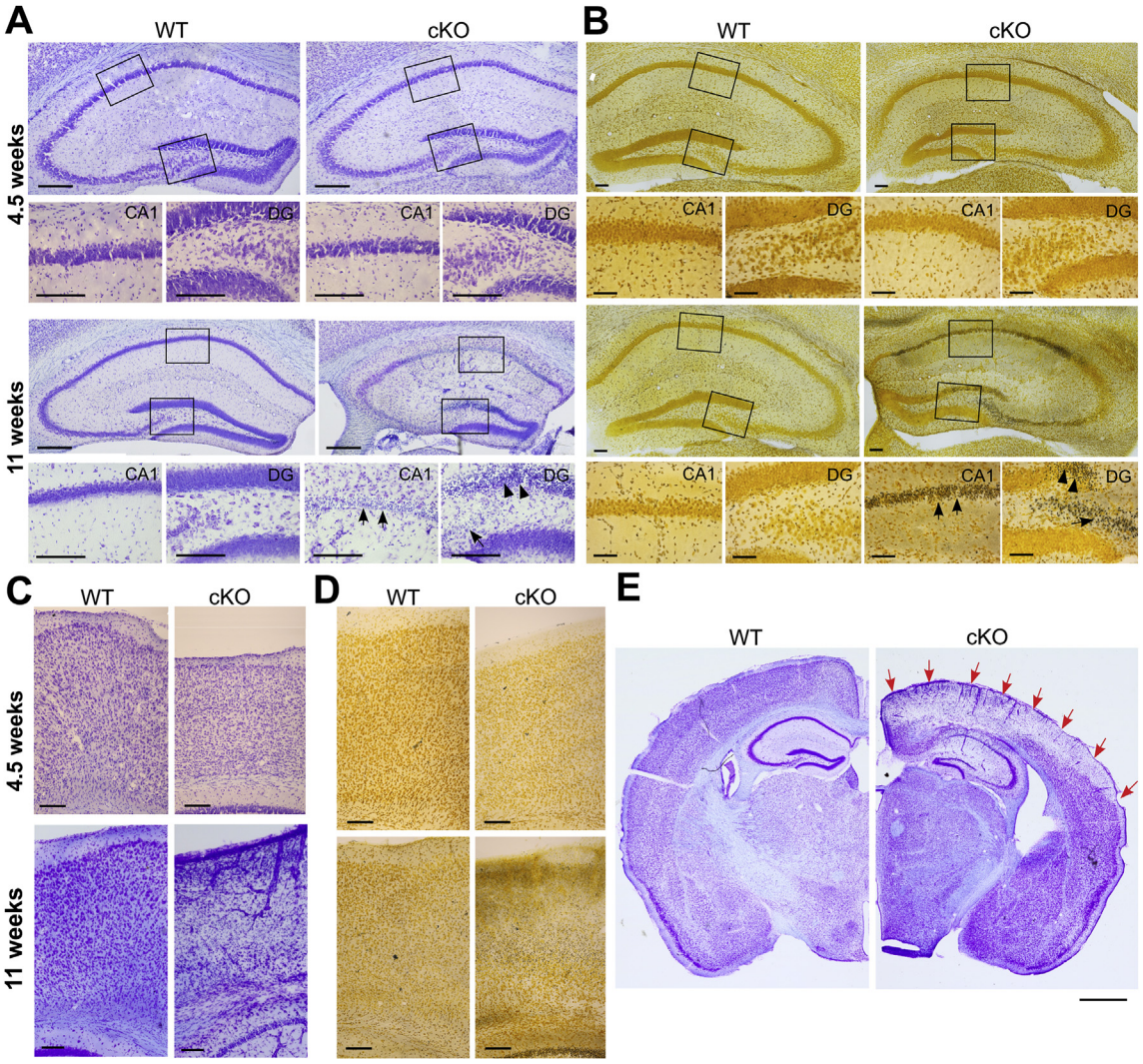

Fig. 4. Mice lacking Glul in the cerebral cortex had progressive neurodegeneration. Nissl (**A**) and NeuroSilver (**B**) staining of hippocampus of WT and cKO mice showed massive neuronal degenerations (arrows) in CA1, in CA3, in part of the granule cell layer and in the hilus of the dentate gyrus (DG) at 11 weeks of age, but not at 4.5 weeks. (**C**) Nissl and (**D**) Neurosilver staining of motor cortex of Glul wildtype and conditional knockouts (cKO) showing massive neuronal degenerations in upper layer of cortex at 9 weeks of age. No neuron degenerations were seen at 4–5 weeks of age. (**E**) Selective degeneration in some areas of cortex indicated by red arrows. Scale bar: 50 μm (**A-D**); 1 mm (**E**).

obvious neuropathological changes started in the hippocampus, as evidenced by selective degeneration of CA1 and CA3 pyramidal neurons and dentate granule cells. The hippocampal pathology occurred bilaterally and was readily apparent in the third postnatal month (Fig. 4AB). As the mice aged further, the neocortex became progressively affected in multiple areas, particularly the retrosplenial, motor, somatosensory, parietal association and visual cortices (Fig. 4C–E). The degree and pattern of neocortical neurodegeneration varied among animals at similar ages, but generally started in the most superficial layer of the cortex (data not shown). Neuro-Silver staining at 11 weeks of age (Fig. 4BD) confirmed that large numbers of neurons were degenerating in the cKO mice, but not in the conditional heterozygotes (Emx1-Cre$^{+/0}$;Glul$^{f/w}$) and the WT (Cre negative) mice.

3.4. Astrocytes lacking Glul become reactive prior to neuronal loss and epilepsy

Considering that Glul is an astrocytic protein, we assessed for reactive astrogliosis by examining the expression of glial fibrillary acid protein (GFAP). Western blotting revealed that the protein was hardly increased in cKO mice versus WT littermates at 2 weeks of age (Fig. 5B), but showed significant increases at 4 weeks of age, consistent with progressive astrogliosis. The increase in GFAP was confirmed by Taqman RT-PCR (data not shown) and immunocytochemistry (Fig. 5A).

3.5. Loss of Glul impacts the molecular anatomy and physiology of cerebral blood vessels

Interestingly, the expression of GFAP was increased in astroglial processes along blood vessels in the cKO mice as early as 3 weeks of age (Fig. 6AB). Further, at later stages, the vessels became markedly dilated in the areas of the neocortex and of the hippocampus where neurodegeneration was occurring. (Fig. 6C). We therefore asked whether the astroglial reactivity was associated with changes in the physiology of cerebral blood vessels. MRI cerebrovascular reactivity (CVR), defined as the relative increase in Blood Oxygen Level Dependent (BOLD) signal during a CO_2 challenge, revealed significant differences between WT and cKO mice at 4 weeks and 12–15 weeks of age (Fig. 6D). In both age groups, CVR was reduced in neocortical areas, such as cingulate and sensorimotor cortices in the cKO mice (4 weeks: WT, 5.44 ± 0.65%; cKO, 2.8 ± 0.58%; 12–15 weeks: WT, 5.65 ± 1.17%; cKO, 1.67 ± 0.44%). In the dorsal hippocampus, a reduction of CVR was

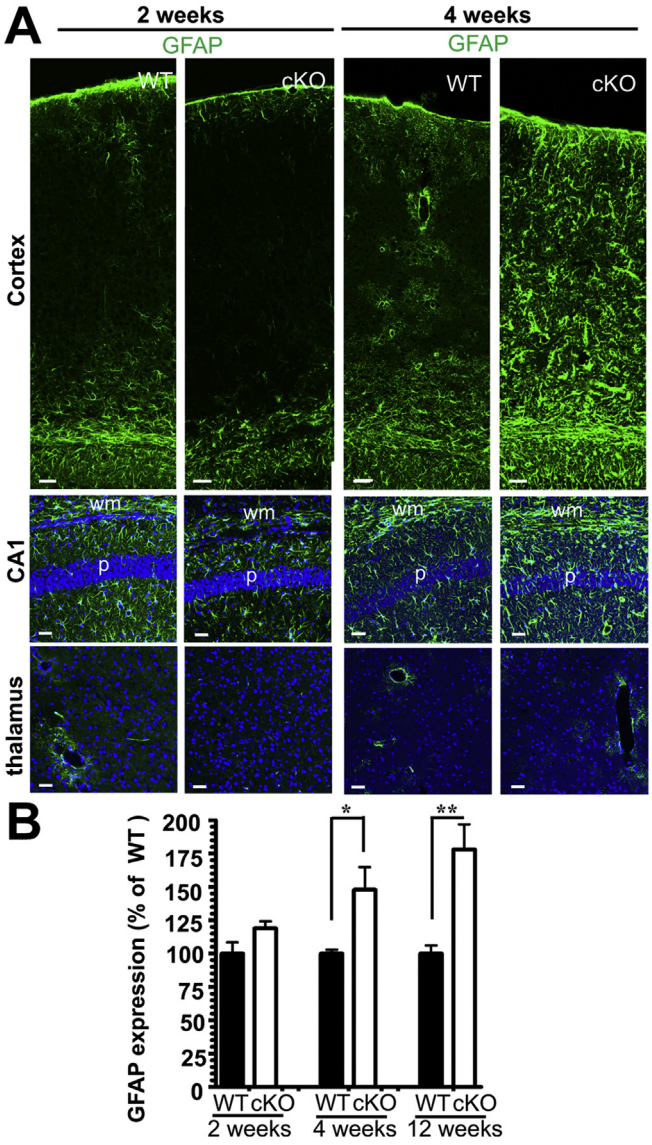

Fig. 5. Lack of cortical Glul leads to astrogliosis preceding neurodegeneration. (**A**) Sections from the neocortex of WT and cKO mice (littermates processed in parallel; ages as indicated) were probed with antibodies to GFAP (green; labels astrocytes). Astrogliosis, as indicated by increased GFAP expression, was evident in the neocortex and hippocampus CA1 of 4 weeks old cKO mice. In contrast, thalamus in the cKO (where Emx1-Cre is not active) showed normal expression of GFAP at both age groups. Scale bar 50 μm. (**B**) GFAP expression increases with age being statistically significantly increased at four weeks of age. The expression levels were quantified by immunoblotting of hippocampi from wild-type (WT) and Glul cortical knockout (cKO) mice: five pairs of WT and cKO littermates in each age group: 2 weeks of age n = 5 pairs: 3 pairs of males, 2 pairs of females; 4 weeks of age n = 5 pairs: 2 pairs of males, 3 pairs of females; > 12 weeks of age n = 5 pairs: 4 pairs of males, 1 pair of females; *p < 0.05, **p < 0.01.

noted at 4 weeks of age in the cKO mice, but not at 12–15 weeks of age (4 weeks: WT, 4.37 ± 0.75%; cKO, 2.24 ± 0.35%; 12–15 weeks: WT, 3.35 ± 0.37%; cKO, 3.03 ± 0.33%). In subcortical areas spared from Glul deletion like the basal forebrain, no significant group effect was found at either age (4 weeks: WT, 3.22 ± 0.59%; cKO, 2.81 ± 0.41%; 12–15 weeks: WT, 2.39 ± 0.37%; cKO, 2.88 ± 0.46%).

3.6. Young mice lacking cortical Glul have abnormal glutamate signaling

As Glul is critical for the homeostasis of glutamate, glutamine and GABA, and as cerebral blood flow is regulated through glutamate-mediated astrocyte responses (Attwell et al., 2010), we quantified the levels of these and other amino acids in the cKO and WT brains (Table 1). As expected, the concentrations of glutamine, glutamate, aspartate and GABA in the tissue were significantly lower in the cKO cortex than in the WT cortex, whereas no changes were observed in the cerebellum, which expressed normal levels of Glul (Fig. 1BC).

We also assessed several molecules involved in glutamate signaling by Taqman RT-PCR (Fig. 7A) and found reduced levels of mRNA encoding the major glial glutamate transporter EAAT2 and of mRNA encoding the glutamate receptor subunits GRIA1 (GluR1) and GRIN2A (GluN2A) in the hippocampi of 5 weeks old cKO mice. Immunoblotting of EAAT2 showed that the reduction in EAAT2 protein levels was present already at 2 weeks of age (Fig. 7B). Another glial glutamate transporter, EAAT1, displayed a similar expression pattern albeit less pronounced, while the expression of EAAT3 (which is the major neuronal glutamate transporter at the plasma membrane: Holmseth et al., 2012b) and neuronal vesicular glutamate transporter VGluT1 were not changed significantly.

4. Discussion

The exact role of Glul in the etiology of CNS disease, including epilepsy, is poorly understood due to the lack of viable and specific *in vivo* approaches. To overcome this hurdle, we selectively deleted Glul in the cerebral cortex of mice. This resulted in a viable Glul knockout model and proved that a selective loss of cortical Glul is, by itself, sufficient to cause epileptic seizures and progressive neurodegeneration resembling hippocampal sclerosis. The mutation had a high penetrance considering that the C57BL6 mouse strain used here is relatively resistant to epileptic seizures (McLin and Steward, 2006).

However, the first behavioral seizures or neurodegeneration were only evident in animals six weeks of age or older, even though changes in brain chemistry, glial cells and cortical blood vessels had been present for several weeks. Thus, seizures and neurodegeneration are likely not directly caused by the Glul deficiency, but rather occur as a consequence of a pathological process involving reactive astrocytes and impaired neurovascular coupling. These slowly developing effects of Glul deficiency are distinctly different from the rapid, excitotoxic syndrome with early seizures and increased mortality seen in EAAT2 knockout mice (Tanaka et al., 1997; Zhou et al., 2014).

It is well known that brain tissues from humans with epilepsy and from animal models of the disease contain reactive astrocytes and altered blood vessels (Eyo et al., 2017; Wolf et al., 2017). While these changes were originally regarded as secondary responses to injury, more recent studies have shown that reactive astrocytes can induce neuronal hyperexcitability and spontaneous seizures irrespective of the primary initiating event (Ortinski et al., 2010; Robel et al., 2015). In line with this gliopathy hypothesis of epilepsy (Verkhratsky et al., 2012; Coulter and Eid, 2012; Robel and Sontheimer, 2016), we observed reactive astrocytes weeks before the first seizure and neuron loss were detected.

Further, astrocytes, particularly their cytoplasmic processes, are integral elements of the neurovascular unit and can control vessel diameter (Attwell et al., 2010). Numerous changes in the molecular anatomy of microvessels in Glul-deficient brain regions in patients with TLE and animal models of the disorder have been demonstrated (Eid et al., 2016). However, whether these changes are a cause or consequence of seizures has remained unclear. Here we show, for the first time, that deletion of astrocytic Glul leads to increased vascular caliber and lack of vasodilation in response to CO_2. These changes were present *before* the occurrence of seizures and significant neuron loss, and were probably induced by dysfunctional glutamate-ammonia handling as the only known reaction catalyzed by Glul is the production of glutamine; a process which also results in inactivation of glutamate and detoxification of ammonia (Eid et al., 2016). Here we demonstrated that deletion

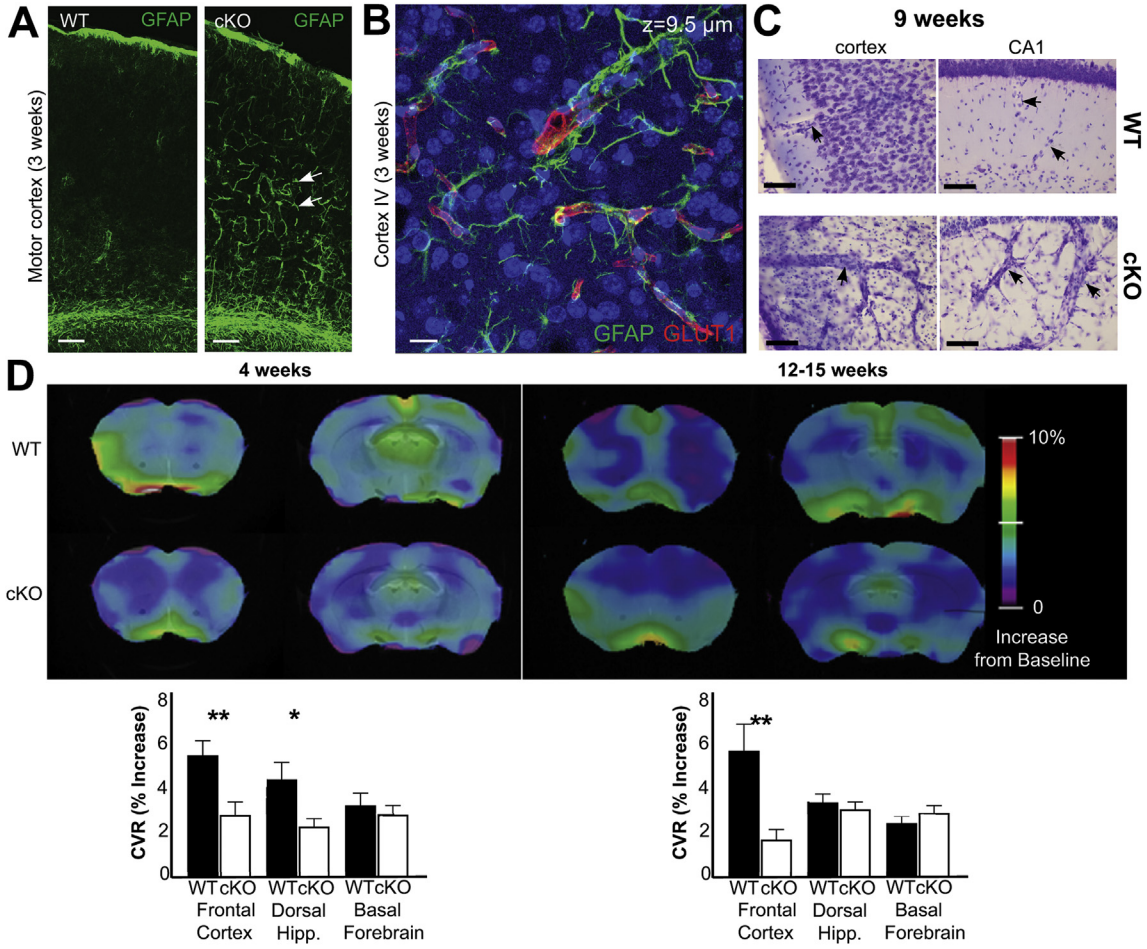

Fig. 6. Glul knockout mice (cKO) had altered cerebral blood vessels with reduced ability to react to increases in CO_2 levels. **(A)** There was increased GFAP labeling (green) in astroglial processes in 3 weeks old Glul cKO mice. The images from wildtype (WT) and cKO mice represent montages of three overlapping images acquired from the motor cortex. Scale bar 100 µm. **(B)** Z-stack image (total thickness 9.5 µm) acquired from motor cortex (layer VI) of the same cKO section as in **A**. Note increased GFAP labeling in astroglial processes surrounding blood vessels (red, GLUT1). Scale bar 100 µm. **(C)** Nissl staining shows changed vascular structures in the motor cortex and hippocampus CA1 of 9 weeks old cKO mice compared to WT littermates (processed in parallel). Scale bar 50 µm. **(D)** Impaired cerebrovascular reactivity in (as indicated) 4 and 12–15 weeks old cKO mice. Voxel-level maps of cerebrovascular reactivity (CVR), as defined by the relative increase of signal during CO_2 challenge, averaged across each age/group. Maps are projected on two coronal slices of a structural mouse atlas. Region of interest-averaged CVR amplitudes are shown on bar graphs (bottom); cKO mice have impaired CVR response in the dorsal hippocampus at 12 weeks, and in the cortex at both time-points. Subcortical areas like the basal forebrain are unaffected in cKO animals. The most cranial slices (the left images on each sub-figure) are +1.2 mm from bregma, while the caudal slices (the right images on each sub-figure) are −0.6 mm from bregma. *p < 0.05; **p < 0.01.

of Glul causes a major reduction in brain tissue levels of glutamine, glutamate and GABA. The reductions in glutamate and GABA probably reflect decreases in the neuronal transmitter pool as most tissue glutamate and GABA is in neurons (Danbolt, 2001). When glutamate cannot be amidated to glutamine, due to lack of Glul, glutamate is likely degraded via the glial tricarboxylic acid cycle rather than being transferred back to neurons as glutamine. Because glutamine is a precursor for the synthesis of neuronal glutamate and GABA, the lack of glutamine in the cKO cortex probably explains the low levels of the neurotransmitters. However, it is important to note that neurons may be able to synthesize glutamate *de novo* (Hassel and Bråthe, 2000) and that glutamate transporters in axon-terminals represent a mechanism for direct recycling independent of Glul (Danbolt et al., 2016b; Zhou et al., 2018). This may explain why *in vitro* electrophysiological recordings show that axon-terminals can maintain basal glutamatergic neurotransmission during low extracellular glutamine conditions, whereas glutamine was only required for sustained high-frequency firing (Tani et al., 2014). A reduction in total tissue glutamate does not necessarily indicate decreased extracellular glutamate. The episodes of wild-running and the occurrence of seizures in the Glul cKO mice are, however, suggestive of hyperexcitability, which may indicate increased extracellular glutamate. In support, these cKO mice have reductions in expression of glutamate transporters (EAAT1 and EAAT2), but these were moderate. Other factors that may contribute to increased excitability comprise reduced GABA levels and reductions in the GRIN2A glutamate receptor subunit. In addition, a conceptually distinct pathway of the control of cerebral blood flow mediated by glutamate transporters has been suggested, though it is unclear at the moment whether it is a direct or indirect effect (Petzold et al., 2008; Schummers et al., 2008). Further, the brain has no urea cycle, and detoxification of ammonia by Glul is thereby the only significant mechanism apart from removal via blood. Consequently, Glul deficiency probably raises ammonia levels. The similarity between the ammonium ion and the potassium ion implies that ammonium ions can impair potassium buffering by interfering with several transporter proteins and subsequently weaken neuronal inhibition (Rangroo Thrane et al., 2013). A raised $[K^+]$ could affect the function of smooth muscle via inward rectifier K^+ channels and dilates the vessels (Knot et al., 1996). In conclusion, there are several factors that are likely to increase excitability, but we do not at this stage know their relative importance.

Even though the Glul cKO mice replicate several features of human TLE, there are notable differences. First, the mice are deficient in Glul in

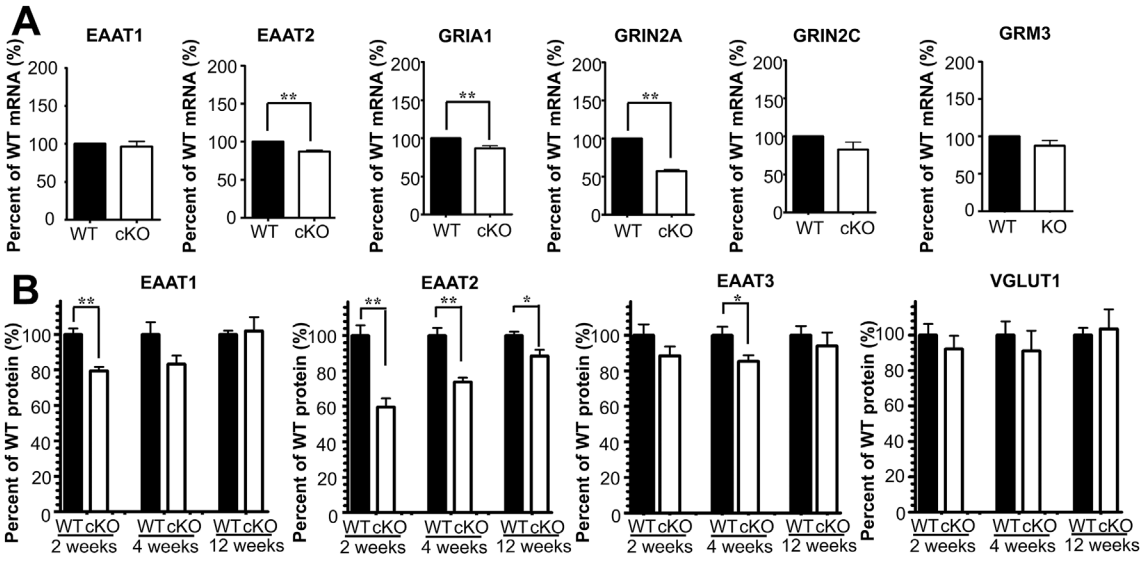

Fig. 7. Several of the components of the glutamatergic signaling system were altered in Glul cortical knockout (cKO) mice. (**A**) Taqman RT-PCR revealed statistically significant reductions in the expression of glutamate transporter EAAT2 (**p < 0.01) and of the glutamate receptor subunits GRIA1 (**p < 0.01) and GRIN2A (**p < 0.01) in the hippocampi of 5 weeks old cKO mice compared to their wild-type (WT) littermates (n = 4 pairs of male mice). In contrast, the expression of GRIN2C (p = 0.119), GRM3 (p = 0.128) and EAAT1 (p = 0.606) were not changed. The expression levels were normalized with that of GAPDH (control). (**B**) Immunoblots showed statistically significant (*p < 0.05; **p < 0.01) reduction in expression of glutamate transporter proteins in the hippocampus of young cKO mice compared to their WT littermates (2 weeks of age n = 5 pairs: 3 pairs of males, 2 pairs of females; 4 weeks of age n = 5 pairs: 2 pairs of males, 3 pairs of females; > 12 weeks of age n = 5 pairs: 4 pairs of males, 1 pair of females). Note that EAAT2 was the most affected subtype and that the strongest reduction was in the youngest mice. In contrast, the vesicular glutamate transporter 1, VGLUT1, was hardly reduced (n = 3 pairs of WT and cKO mice).

large portions of the cerebral cortex from early embryonic life, whereas patients with MTLE exhibit focal losses of Glul in the hippocampus and amygdala (Eid et al., 2004; van der Hel et al., 2005). Moreover, the Glul loss in human MTLE is probably not present during embryogenesis, but likely occurs secondary to another insult, later in life. Despite these differences, we have clearly demonstrated that loss of Glul in the cerebral cortex leads to epilepsy and progressive neurodegeneration, which are key features of human MTLE. We have also shown that loss of astrocytic Glul leads to significant changes in cerebrovascular physiology, suggesting new and important roles of Glul in neurovascular biology.

5. Conclusions

In summary, Glul deficiency does not immediately lead to seizures via a classical excitotoxic syndrome, but rather triggers a prolonged pathological process involving early glial and cerebrovascular changes before progressive neuron loss become apparent.

Author contribution statement

YZ and NCD designed the research; YZ managed the mouse colony, performed histological staining, immunocytochemistry, immunoblots and behavioral testing; RD and SEG performed the video-EEG recordings; MP performed the brain imaging; HQX carried out histological staining and analyzed open field behavioral videos; BH quantified amino acids; YSP generated the Glul-flox mice; YZ, TE and NCD wrote the manuscript. All authors approved the final manuscript.

Conflicts of interest

The authors declare no competing financial interests.

Acknowledgements

We are grateful to the staff at the animal facility at The Norwegian Governmental Institute of Public Health for assisting with animal husbandry. This study was supported by the Norwegian Research Council (Grant no. 240844 to NCD), Novo Nordisk Fonden (Grant no. NNF14OC0010959 and NNF15OC0016528 to NCD), University of Oslo (SERTA to NCD; UNIFOR-FRIMED to NCD; PhD fellowship to HQX), and the National Institutes of Health (NIH, Grants number NS070824 to TE, RD and SEG; and MH067528 and NS052519 to FH). This work was also made possible by a grant from the National Center for Advancing Translational Sciences (NCATS; UL1 TR000142), a component of the NIH and the NIH Roadmap for Medical Research.

References

Attwell, D., Buchan, A.M., Charpak, S., Lauritzen, M., Macvicar, B.A., Newman, E.A., 2010. Glial and neuronal control of brain blood flow. Nature 468, 232–243.
Bernard-Helary, K., Ardourel, M.-Y., Hevor, T., Cloix, J.-F., 2002. In vivo and in vitro glycogenic effects of methionine sulfoximine are different in two inbred strains of mice. Brain Res. 929, 147–155.
Blumenfeld, H., Varghese, G.I., Purcaro, M.J., Motelow, J.E., Enev, M., McNally, K.A., Levin, A.R., Hirsch, L.J., Tikofsky, R., Zubal, I.G., Paige, A.L., Spencer, S.S., 2009. Cortical and subcortical networks in human secondarily generalized tonic-clonic seizures. Brain 132, 999–1012.
Coulter, D.A., Eid, T., 2012. Astrocytic regulation of glutamate homeostasis in epilepsy. Glia 60, 1215–1226.
Dahlberg, D., Ivanovic, J., Hassel, B., 2014. High extracellular concentration of excitatory amino acids glutamate and aspartate in human brain abscess. Neurochem. Int. 69, 41–47.
Danbolt, N.C., 2001. Glutamate uptake. Prog. Neurobiol. 65, 1–105.
Danbolt, N.C., Furness, D.N., Zhou, Y., 2016b. Neuronal vs glial glutamate uptake: resolving the conundrum. Neurochem. Int. 98, 29–45.
Danbolt, N.C., Lehre, K.P., Dehnes, Y., Chaudhry, F.A., Levy, L.M., 1998. Localization of transporters using transporter-specific antibodies. Methods Enzymol. 296, 388–407.
Danbolt, N.C., Zhou, Y., Furness, D.N., Holmseth, S., 2016a. Strategies for immunohistochemical protein localization using antibodies: what did we learn from neurotransmitter transporters in glial cells and neurons. Glia 64, 2045–2064.
Eid, T., Ghosh, A., Wang, Y., Beckstrom, H., Zaveri, H.P., Lee, T.-S.W., Lai, J.C., Malthankar-Phatak, G.H., de Lanerolle, N.C., 2008. Recurrent seizures and brain pathology after inhibition of glutamine synthetase in the hippocampus in rats. Brain 131, 2061–2070.
Eid, T., Gruenbaum, S.E., Dhaher, R., Lee, T.-S.W., Zhou, Y., Danbolt, N.C., 2016. The glutamate-glutamine cycle in epilepsy. In: Schousboe, A., Sonnewald, U. (Eds.), The Glutamate/GABA-Glutamine Cycle - Amino Acid Neurotransmitter Homeostasis. Springer International Publishing, Switzerland.
Eid, T., Thomas, M.J., Spencer, D.D., Rundenpran, E., Lai, J.C.K., Malthankar, G.V., Kim, J.H., Danbolt, N.C., Ottersen, O.P., Delanerolle, N.C., 2004. Loss of glutamine

synthetase in the human epileptogenic hippocampus: possible mechanism for raised extracellular glutamate in mesial temporal lobe epilepsy. Lancet 363, 28–37.
Eyo, U.B., Murugan, M., Wu, L.-J., 2017. Microglia-neuron communication in epilepsy. Glia 65, 5–18.
Ferguson, R.E., Carroll, H.P., Harris, A., Maher, E.R., Selby, P.J., Banks, R.E., 2005. Housekeeping proteins: a preliminary study illustrating some limitations as useful references in protein expression studies. Proteomics 5, 566–571.
Gorski, J.A., Talley, T., Qiu, M., Puelles, L., Rubenstein, J.L., Jones, K.R., 2002. Cortical excitatory neurons and glia, but not GABAergic neurons, are produced in the Emx1-expressing lineage. J. Neurosci. 22, 6309–6314.
Haberle, J., Shahbeck, N., Ibrahim, K., Schmitt, B., Scheer, I., O'Gorman, R., Chaudhry, F.A., Ben-Omran, T., 2012. Glutamine supplementation in a child with inherited GS deficiency improves the clinical status and partially corrects the peripheral and central amino acid imbalance. Orphanet J. Rare Dis. 7, 48.
Hassel, B., Bråthe, A., 2000. Neuronal pyruvate carboxylation supports formation of transmitter glutamate. J. Neurosci. 20, 1342–1347.
He, Y., Hakvoort, T.B., Vermeulen, J.L., Labruyere, W.T., De Waart, D.R., Van Der Hel, W.S., Ruijter, J.M., Uylings, H.B., Lamers, W.H., 2010. Glutamine synthetase deficiency in murine astrocytes results in neonatal death. Glia 58, 741–754.
He, Y., Hakvoort, T.B., Vermeulen, J.L., Lamers, W.H., Van Roon, M.A., 2007. Glutamine synthetase is essential in early mouse embryogenesis. Dev. Dynam. 236, 1865–1875.
Holmseth, S., Dehnes, Y., Huang, Y.H., Follin-Arbelet, V.V., Grutle, N.J., Mylonakou, M.N., Plachez, C., Zhou, Y., Furness, D.N., Bergles, D.E., Lehre, K.P., Danbolt, N.C., 2012b. The density of EAAC1 (EAAT3) glutamate transporters expressed by neurons in the mammalian CNS. J. Neurosci. 32, 6000–6013.
Holmseth, S., Scott, H.A., Real, K., Lehre, K.P., Leergaard, T.B., Bjaalie, J.G., Danbolt, N.C., 2009. The concentrations and distributions of three C-terminal variants of the GLT1 (EAAT2; slc1a2) glutamate transporter protein in rat brain tissue suggest differential regulation. Neuroscience 162, 1055–1071.
Holmseth, S., Zhou, Y., Follin-Arbelet, V.V., Lehre, K.P., Bergles, D.E., Danbolt, N.C., 2012a. Specificity controls for immunocytochemistry: the antigen pre-adsorption test can lead to inaccurate assessment of antibody specificity. J. Histochem. Cytochem. 60, 174–187.
Kam, K., Nicoll, R., 2007. Excitatory synaptic transmission persists independently of the glutamate-glutamine cycle. J. Neurosci. 27, 9192–9200.
Knot, H.J., Zimmermann, P.A., Nelson, M.T., 1996. Extracellular K(+)-induced hyperpolarizations and dilatations of rat coronary and cerebral arteries involve inward rectifier K(+) channels. J. Physiol. 492 (Pt 2), 419–430.
Laemmli, U.K., 1970. Cleavage of structural proteins during the assembly of the head of bacteriophage T4. Nature 227, 680–685.
Lee, E.C., Yu, D., Martinez de Velasco, J., Tessarollo, L., Swing, D.A., Court, D.L., Jenkins, N.A., Copeland, N.G., 2001. A highly efficient Escherichia coli-based chromosome engineering system adapted for recombinogenic targeting and subcloning of BAC DNA. Genomics 73, 56–65.
Lehre, K.P., Levy, L.M., Ottersen, O.P., Storm-Mathisen, J., Danbolt, N.C., 1995. Differential expression of two glial glutamate transporters in the rat brain: quantitative and immunocytochemical observations. J. Neurosci. 15, 1835–1853.
Li, Y., Zhou, Y., Danbolt, N.C., 2012. The rates of postmortem proteolysis of glutamate transporters differ dramatically between cells and between transporter subtypes. J. Histochem. Cytochem. 60, 811–821.
Lowry, O.H., 1953. The quantitative histochemistry of the brain. J. Histochem. Cytochem. 1, 420–428.
Lowry, O.H., Roberts, N.R., Leiner, K.Y., Wu, M.L., Farr, A.L., Albers, R.W., 1954. The quantitative histochemistry of brain, III. ammon's horn. J. Biol. Chem. 207, 39–49.
Lowry, O.H., Rosebrough, N.J., Farr, A.L., Randall, R.J., 1951. Protein measurement with the Folin phenol reagent. J. Biol. Chem. 193, 265–275.
Martinez-Hernandez, A., Bell, K.P., Norenberg, M.D., 1977. Glutamine synthetase: glial localization in brain. Science 195, 1356–1358.
McLin, J.P., Steward, O., 2006. Comparison of seizure phenotype and neurodegeneration induced by systemic kainic acid in inbred, outbred, and hybrid mouse strains. Eur. J. Neurosci. 24, 2191–2202.
Ortinski, P.I., Dong, J., Mungenast, A., Yue, C., Takano, H., Watson, D.J., Haydon, P.G., Coulter, D.A., 2010. Selective induction of astrocytic gliosis generates deficits in neuronal inhibition. Nat. Neurosci. 13, 584–591.
Petzold, G.C., Albeanu, D.F., Sato, T.F., Murthy, V.N., 2008. Coupling of neural activity to blood flow in olfactory glomeruli is mediated by astrocytic pathways. Neuron 58, 897–910.
Racine, R.J., Burnham, W.M., Gartner, J.G., Levitan, D., 1973. Rates of motor seizure development in rats subjected to electrical brain stimulation: strain and inter-stimulation interval effects. Electroencephalogr. Clin. Neurophysiol. 35, 553–556.
Rangroo Thrane, V., Thrane, A.S., Wang, F., Cotrina, M.L., Smith, N.A., Chen, M., Xu, Q., Kang, N., Fujita, T., Nagelhus, E.A., Nedergaard, M., 2013. Ammonia triggers neuronal disinhibition and seizures by impairing astrocyte potassium buffering. Nat. Med. 19, 1643–1648.
Robel, S., Buckingham, S.C., Boni, J.L., Campbell, S.L., Danbolt, N.C., Riedemann, T., Sutor, B., Sontheimer, H., 2015. Reactive astrogliosis causes the development of spontaneous seizures. J. Neurosci. 35, 3330–3345.
Robel, S., Sontheimer, H., 2016. Glia as drivers of abnormal neuronal activity. Nat. Neurosci. 19, 28–33.
Schummers, J., Yu, H., Sur, M., 2008. Tuned responses of astrocytes and their influence on hemodynamic signals in the visual cortex. Science 320, 1638–1643.
Shaw, C.A., Bains, J.S., 2002. Synergistic versus antagonistic actions of glutamate and glutathione: the role of excitotoxicity and oxidative stress in neuronal disease. Cell. Mol. Biol. 48, 127–136.
Soriano, P., 1997. The PDGF alpha receptor is required for neural crest cell development and for normal patterning of the somites. Development 124, 2691–2700.
Spodenkiewicz, M., Diez-Fernandez, C., Rufenacht, V., Gemperle-Britschgi, C., Haberle, J., 2016. Minireview on glutamine synthetase deficiency, an ultra-rare inborn error of amino acid biosynthesis. Biology (Basel) 5, 40.
Tanaka, K., Watase, K., Manabe, T., Yamada, K., Watanabe, M., Takahashi, K., Iwama, H., Nishikawa, T., Ichihara, N., Kikuchi, T., Okuyama, S., Kawashima, N., Hori, S., Takimoto, M., Wada, K., 1997. Epilepsy and exacerbation of brain injury in mice lacking the glutamate transporter GLT-1. Science 276, 1699–1702.
Tani, H., Dulla, C.G., Farzampour, Z., Taylor-Weiner, A., Huguenard, J.R., Reimer, R.J., 2014. A local glutamate-glutamine cycle sustains synaptic excitatory transmitter release. Neuron 81, 888–900.
van der Hel, W.S., Notenboom, R.G., Bos, I.W., van Rijen, P.C., van Veelen, C.W., de Graan, P.N., 2005. Reduced glutamine synthetase in hippocampal areas with neuron loss in temporal lobe epilepsy. Neurology 64, 326–333.
Verkhratsky, A., Sofroniew, M.V., Messing, A., deLanerolle, N.C., Rempe, D., Rodriguez, J.J., Nedergaard, M., 2012. Neurological diseases as primary gliopathies: a reassessment of neurocentrism. ASN Neuro 44, e00082.
Wolf, S.A., Boddeke, H.W., Kettenmann, H., 2017. Microglia in physiology and disease. Annu. Rev. Physiol. 79, 619–643.
Wurst, W., Joyner, A.L., 1999. In: Targeting, Gene, Practical Approach, A., Joyner, A.L. (Eds.), Production of Targeted Embryonic Stem Cell Clones. Oxford University Press, New York.
Zhou, Y., Hassel, B., Eid, T., Danbolt, N.C., 2018. Axon-terminals expressing EAAT2 (GLT-1; Slc1a2) are common in the forebrain and not limited to the hippocampus. Neurochem. Int (in press).
Zhou, Y., Holmseth, S., Hua, R., Lehre, A.C., Olofsson, A.M., Poblete-Naredo, I., Kempson, S.A., Danbolt, N.C., 2012. The betaine-GABA transporter (BGT1, slc6a12) is predominantly expressed in the liver and at lower levels in the kidneys and at the brain surface. Am. J. Physiol. Ren. Physiol. 302, F316–F328.
Zhou, Y., Waanders, L.F., Holmseth, S., Guo, C., Berger, U.V., Li, Y., Lehre, A.-C., Lehre, K.P., Danbolt, N.C., 2014. Proteome analysis and conditional deletion of the EAAT2 glutamate transporter provide evidence against a role of EAAT2 in pancreatic insulin secretion in mice. J. Biol. Chem. 289, 1329–1344.